Distinct Patterns of Constitutive Phosphodiesterase Activity in Mouse Sinoatrial Node and Atrial Myocardium

Rui Hua[⬩], Andrew Adamczyk[⬩], Courtney Robbins, Gibanananda Ray, Robert A. Rose*

Department of Physiology and Biophysics, Faculty of Medicine, Dalhousie University, Halifax, Nova Scotia, Canada

Abstract

Phosphodiesterases (PDEs) are critical regulators of cyclic nucleotides in the heart. In ventricular myocytes, the L-type Ca^{2+} current ($I_{Ca,L}$) is a major target of regulation by PDEs, particularly members of the PDE2, PDE3 and PDE4 families. Conversely, much less is known about the roles of PDE2, PDE3 and PDE4 in the regulation of action potential (AP) properties and $I_{Ca,L}$ in the sinoatrial node (SAN) and the atrial myocardium, especially in mice. Thus, the purpose of our study was to measure the effects of global PDE inhibition with Isobutyl-1-methylxanthine (IBMX) and selective inhibitors of PDE2, PDE3 and PDE4 on AP properties in isolated mouse SAN and right atrial myocytes. We also measured the effects of these inhibitors on $I_{Ca,L}$ in SAN and atrial myocytes in comparison to ventricular myocytes. Our data demonstrate that IBMX markedly increases spontaneous AP frequency in SAN myocytes and AP duration in atrial myocytes. Spontaneous AP firing in SAN myocytes was also increased by the PDE2 inhibitor erythro-9-[2-hydroxy-3-nonyl] adenine (EHNA), the PDE3 inhibitor milrinone (Mil) and the PDE4 inhibitor rolipram (Rol). In contrast, atrial AP duration was increased by EHNA and Rol, but not by Mil. IBMX also potently, and similarly, increased $I_{Ca,L}$ in SAN, atrial and ventricular myocytes; however, important differences emerged in terms of which inhibitors could modulate $I_{Ca,L}$ in each myocyte type. Consistent with our AP measurements, EHNA, Mil and Rol each increased $I_{Ca,L}$ in SAN myocytes. Also, EHNA and Rol, but not Mil, increased atrial $I_{Ca,L}$. In complete contrast, no selective PDE inhibitors increased $I_{Ca,L}$ in ventricular myocytes when given alone. Thus, our data show that the effects of selective PDE2, PDE3 and PDE4 inhibitors are distinct in the different regions of the myocardium indicating important differences in how each PDE family constitutively regulates ion channel function in the SAN, atrial and ventricular myocardium.

Introduction

Phosphodiesterases (PDEs) are phosphohydrolase enzymes that are responsible for the degradation of the cyclic nucleotides adenosine and guanosine $3',5'$ cyclic monophosphate (cAMP and cGMP) [1,2]. PDEs play critical roles in the modulation of cellular functions that depend on cAMP and cGMP in the heart, including electrical conduction, contractility, metabolism and transcription [3], by controlling the levels of these powerful signaling molecules in cells. PDEs exist in 11 families (PDE1-11) with several isoforms in each and are regulated by diverse mechanisms including phosphorylation, binding of cyclic nucleotides, calcium binding and protein-protein interactions [1]. With such a large number of families and isoforms PDE signaling is clearly complex and in this context it is now thought that PDEs are importantly involved in the compartmentation of cyclic nucleotide signaling whereby the subcellular localization of different PDE isoforms can lead to distinct spatial and temporal pools of cAMP and/or cGMP [3–6]. This can result in distinct roles for specific PDEs in different parts of the cell or in different conditions.

Among the PDE families expressed in the heart [7] PDE2, PDE3 and PDE4 have been shown to contribute substantially to cyclic nucleotide regulation, especially in the context of modulating ion channel function [3,4,8,9]. Numerous studies have demonstrated that the L-type Ca^{2+} current ($I_{Ca,L}$) is a critical target of regulation by PDEs in ventricular myocytes. Specifically, it is established that global PDE inhibition with the broad spectrum inhibitor 3-Isobutyl-1-methylxanthine (IBMX) potently increases basal ventricular $I_{Ca,L}$ in mice and rats [8,10,11]. Interestingly, selective inhibition of PDE2, PDE3 or PDE4 alone has no effect on basal $I_{Ca,L}$; however combined inhibition of PDE3 and PDE4 does increase basal $I_{Ca,L}$ and inhibition of PDE2, PDE3 and PDE4 increases basal $I_{Ca,L}$ very similarly to IBMX [8,10,11]. Although the effects of PDE2, 3 and 4 inhibition on $I_{Ca,L}$ have been well characterized in ventricular myocytes much less is known about the role of these PDE families in the sinoatrial node (SAN) and atria, particularly in mice, a very common model organism due to its use in studies incorporating genetic manipulations.
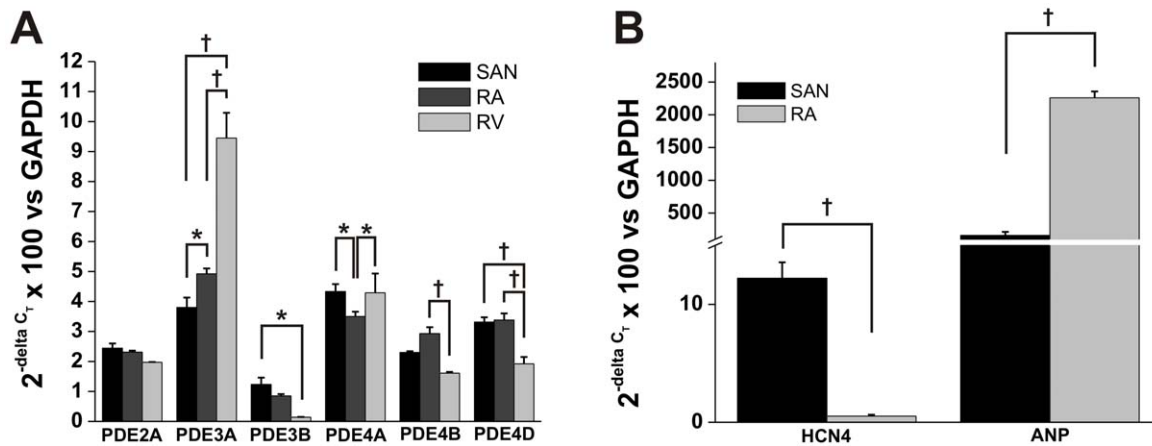
Figure 1. Quantitative mRNA expression of PDE 2, 3 and 4 subtypes in mouse SAN, right atrium and right ventricle. A. Expression of PDE2A, PDE3A, PDE3B, PDE4A, PDE4B and PDE4D are shown relative to GAPDH for the SAN, right atrium (RA) and right ventricular free wall (RV). **B.** SAN samples were distinguished from RA samples by the characteristic pattern of expression of HCN4 and ANP in these regions. SAN tissue shows high expression of HCN4 and low expression of ANP whereas the RA shows very low HCN4 expression and very high ANP expression. Note scale break on Y-axis. Data are means $\pm$ SEM; $n = 5$ SAN trials, 5 right atrial appendage trials and 3 right ventricular free wall trials; *$P < 0.05$; †$P < 0.001$ by two way ANOVA with Tukey's posthoc test.
doi:10.1371/journal.pone.0047652.g001

The SAN contains the specialized pacemaker myocytes whose spontaneous activity is responsible for determining heart rate [12]. Spontaneous action potentials (APs) in these SAN myocytes are characterized by the presence of a diastolic depolarization (DD), during which the SAN myocyte gradually depolarizes until the threshold for an AP is reached [12–14]. Several ionic currents and mechanisms contribute to the generation of the DD including $I_{Ca,L}$ [15]. Consistent with this hypothesis, it has recently been demonstrated that two forms of L-type Ca^{2+} channel, $Ca_V1.2$ and $Ca_V1.3$, contribute to total $I_{Ca,L}$ in SAN myocytes, in contrast to ventricular myocytes which only express $Ca_V1.2$ [16,17]. $Ca_V1.3$ channels activate at more negative membrane potentials than $Ca_V1.2$ enabling them to contribute prominently to the generation of the DD and thereby to the frequency of spontaneous AP firing and heart rate control. $I_{Ca,L}$ is also a critical determinant of AP morphology in working atrial myocytes [18]. Like SAN myocytes, $Ca_V1.2$ and $Ca_V1.3$ both contribute to total $I_{Ca,L}$ in atrial myocytes [19]. Given the unique physiology of the SAN and atria it is possible that PDE regulation of AP properties and ion channels, including $I_{Ca,L}$, is different in these tissues in comparison to the ventricles.

The purpose of this study was to determine the roles of PDE2, PDE3 and PDE4 in regulating AP properties in mouse SAN and atrial myocytes. We also measured the effects of broad spectrum and family specific PDE inhibitors on basal $I_{Ca,L}$ in SAN and atrial myocytes in comparison to ventricular myocytes. This work represents the first direct comparison of these inhibitors on $I_{Ca,L}$ in these three regions of the myocardium in mice. Our data demonstrate that the patterns of constitutive PDE activity are distinct between SAN, atrial and ventricular myocytes, further adding to the complexity of PDE signaling in the heart.

Materials and Methods

Ethics Statement

This study utilized male wildtype C57Bl/6 mice (Charles River) between the ages of 10–14 weeks. Experimental procedures were in accordance with the regulations of The Canadian Council on Animal Care and were approved by The Dalhousie University Committee on Laboratory Animals. In all experiments, mice were anesthetized by isoflurane inhalation and cervically dislocated before hearts were removed.

An expanded Materials and Methods section is available in Appendix S1.

Experimental Approaches

Quantitative mRNA expression for PDE2A, PDE3A, PDE3B, PDE4A, PDE4B and PDE4D in mouse SAN, right atrium and right ventricular free wall was performed using methods we have described previously (see also Appendix S1) [20]. These specific PDE isoforms were selected because our electrophysiological experiments are focused on the PDE2, 3 and 4 families and prior studies [7,11] have shown that the isoforms we measured are expressed in whole ventricular tissue and ventricular myocytes.

Mouse SAN, right atrial and right ventricular myocytes were isolated for patch-clamp recordings using procedures we have described previously [20–23]. Spontaneous and stimulated action potentials (APs) were recorded using the perforated patch-clamp technique in current clamp mode. $I_{Ca,L}$ was recorded in the whole cell patch-clamp configuration. All recordings were performed at room temperature (22–23°C). The solutions and electrophysiological protocols for these experiments are provided in Appendix S1.

Statistics

All summary data are presented as means $\pm$ SEM. Data were analyzed by one or two way ANOVA with Tukey's posthoc analysis or paired Student's t-test. $P < 0.05$ was considered significant.

Results

Region specific mRNA expression of PDE2, 3 and 4 subtypes in the heart

Amongst the PDE2, 3 and 4 families, prior studies have shown that the PDE2A, PDE3A, PDE3B, PDE4A, PDE4B and PDE4D subtypes are expressed in whole ventricular myocardium and/or isolated ventricular myocytes in rodents [7,11]. The relative expression of these PDE isoforms in the SAN and right atrial
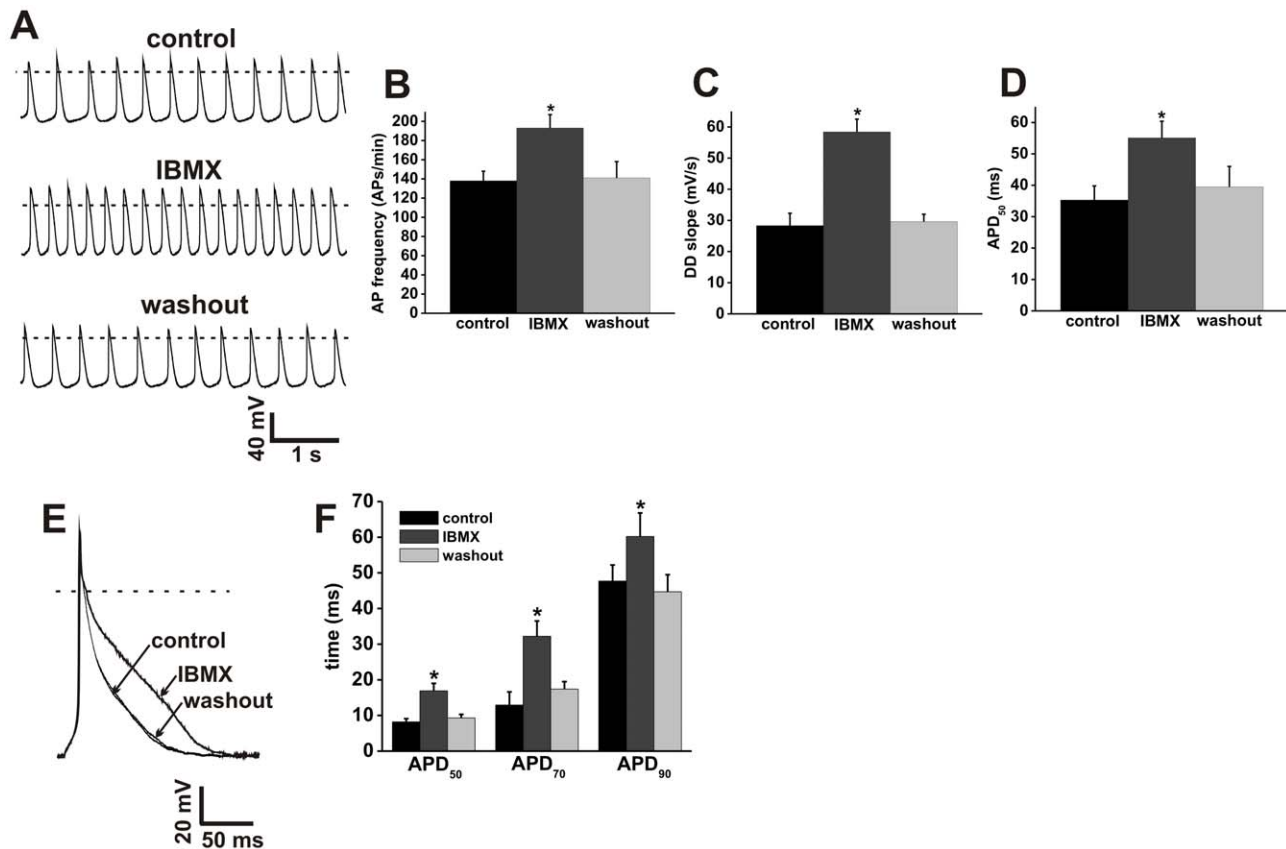
Figure 2. Effects of IBMX on action potential firing in SAN and atrial myocytes. A. Representative spontaneous AP recordings (5 s duration) in control conditions, in the presence of IBMX (100 μM) and after IBMX washout. Dotted lines are at 0 mV. Summary bar graphs illustrate the effects of IBMX on spontaneous AP frequency (**B**), DD slope (**C**) and APD$_{50}$ (**D**). **E.** Representative stimulated right atrial myocyte APs in control conditions, in the presence of IBMX (100 μM) and after IBMX washout. Dotted line is at 0 mV. **F.** Summary of the effects of IBMX on atrial AP duration (APD$_{50}$, APD$_{70}$, and APD$_{90}$). Summary data are means ± SEM; $n = 11$ SAN myocytes and 13 right atrial myocytes; *$P<0.05$ vs. control by one way ANOVA with Tukey's posthoc test.
doi:10.1371/journal.pone.0047652.g002

myocardium; however, have not been determined. Accordingly, we have measured the mRNA expression of PDE2A, PDE3A, PDE3B, PDE4A, PDE4B and PDE4D in the SAN, right atrium and right ventricular free wall using quantitative PCR (Figure 1A). Glyceraldehyde 3-phosphate dehydrogenase (GAPDH) was used as a reference gene. These three regions of myocardium coincide with the cell types used in our electrophysiology experiments (see below). SAN samples were distinguished from right atrial samples based on the high expression of HCN4 and low expression of ANP in the SAN compared to the atrium (Figure 1B) as previously described by us [20] and others [24].

These data demonstrate that each region of the myocardium has a specific pattern of expression for the PDE2, 3 and 4 isoforms we have measured. Specifically, no differences were observed in the expression of PDE2A in each region of the myocardium; however, PDE3A, PDE3B, PDE4A, PDE4B and PDE4D all displayed significant differences in expression between SAN, right atrium and right ventricle as indicated in Figure 1A.

Effects of global PDE inhibition on SAN and right atrial myocyte APs

IBMX is a broad spectrum PDE inhibitor that antagonizes all PDE isoforms [1,11]. In our initial electrophysiological studies we measured the effects of IBMX (100 μM) on spontaneous AP firing in SAN myocytes and stimulated APs in right atrial myocytes

(Figure 2; Tables S1 and S2). IBMX increased ($P<0.05$) spontaneous AP firing in SAN myocytes from 138 ± 10 to 193 ± 14 APs/min with no change in maximum diastolic potential (MDP; Figure 2B, Table S1). This change in AP frequency was associated with increases ($P<0.05$) in DD slope (28.3 ± 4 mV/s in control vs. $58.4\ 4.1$ mV/s in IBMX; Figure 2C) and APD$_{50}$ (35.3 ± 4.5 ms in control vs. 55.1 ± 5.3 ms in IBMX; Figure 2D). Additional SAN AP parameters are shown Table S1, which also shows that the effects of IBMX on SAN myocyte AP firing are fully reversible upon washout.

In right atrial myocytes, IBMX increased ($P<0.05$) AP duration at 50, 70 and 90% repolarization (APD$_{50}$, APD$_{70}$, APD$_{90}$) with no change in resting membrane potential (RMP; Figure 2F, Table S2). Specifically, APD$_{50}$ was increased from 8.2 ± 0.9 to 16.9 ± 2.1 ms, APD$_{70}$ was increased from 12.9 ± 3.7 to 32.2 ± 4.3 ms and APD$_{90}$ was increased from 47.7 ± 4.5 to 60.2 ± 6.6 ms. Additional atrial AP parameters are shown in Table S2. The effects of IBMX on right atrial APs were reversed upon drug washout.

Effects of selective PDE2, PDE3 and PDE4 inhibitors on SAN and right atrial myocyte APs

PDE2, PDE3 and PDE4 have been shown to be major contributors to total PDE activity in rodent ventricular myocytes [10,11]; however, their relative contributions in mouse SAN and
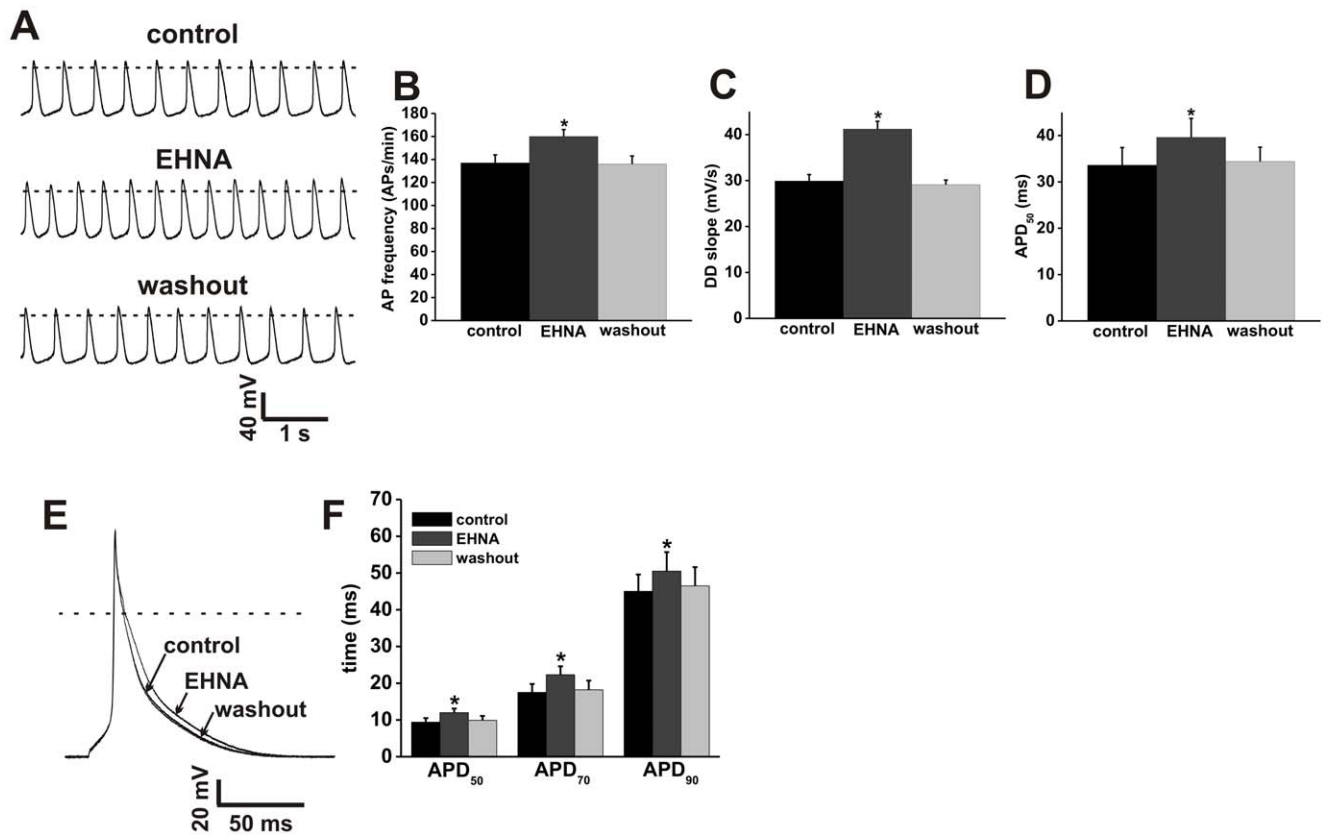
Figure 3. Effects of the PDE2 inhibitor EHNA on action potential firing in SAN and atrial myocytes. A. Representative spontaneous AP recordings (5 s duration) in control conditions, in the presence of EHNA (10 µM) and after EHNA washout. Dotted lines are at 0 mV. Summary bar graphs illustrate the effects of EHNA on spontaneous AP frequency (**B**), DD slope (**C**) and APD_{50} (**D**). **E.** Representative stimulated right atrial myocyte APs in control conditions, in the presence of EHNA (10 µM) and after EHNA washout. Dotted line is at 0 mV. **F.** Summary of the effects of EHNA on atrial AP duration (APD_{50}, APD_{70}, and APD_{90}). Summary data are means ± SEM; $n = 6$ SAN myocytes and 7 right atrial myocytes; $*P < 0.05$ vs. control by one way ANOVA with Tukey's posthoc test.
doi:10.1371/journal.pone.0047652.g003

atrial myocytes are not known. Thus, we next studied the effects of the specific PDE inhibitors erythro-9-[2-hydroxy-3-nonyl]adenine (EHNA; PDE2 inhibitor; 10 µM) [25], milrinone (Mil; PDE3 inhibitor; 10 µM) [10,20] and rolipram (Rol; PDE4 inhibitor; 10 µM) [10]. The selectivity of these inhibitors for specific PDE families is well established, but also concentration dependent. Accordingly, we have used each of these compounds at concentrations that have been previously shown to be selective to their respective PDE family [3,10,11,26,27].

The effects of PDE2 inhibition with EHNA on AP firing in mouse SAN and right atrial myocytes are presented in Figure 3 (see also Tables S3 and S4). EHNA increased ($P < 0.05$) spontaneous AP frequency in SAN myocytes from 137 ± 7 to 160 ± 6 APs/min (Figure 3B). In addition, EHNA increased ($P < 0.05$) DD slope (28.9 ± 1.4 mV/s in control vs. 41.2 mV/s in EHNA; Figure 3C) and APD_{50} (33.6 ± 3.8 ms in control vs. 39.6 ± 4.1 ms in EHNA; Figure 3D). EHNA also increased ($P < 0.05$) AP duration in mouse right atrial myocytes (Figure 3F). Specifically, APD_{50} was increased from 9.4 ± 1.1 to 12 ± 1.1 ms, APD_{70} was increased from 17.5 ± 2.3 to 22.3 ± 2.3 ms and APD_{90} was increased from 45 ± 4.6 to 50.5 ± 5.2 ms. The effects of EHNA were reversed upon washout. These data demonstrate that PDE2 constitutively regulates AP firing in mouse SAN and atrial myocytes in basal conditions.

The effects of the PDE3 inhibitor Mil on AP firing in mouse SAN and right atrial myocytes are illustrated in Figure 4 (see also Tables S5 and S6). Mil increased ($P < 0.05$) spontaneous SAN myocyte AP frequency from 135 ± 6 to 169 ± 6 APs/min (Figure 4B). Mil also increased ($P < 0.05$) DD slope from 28.5 ± 3.4 to 49.9 ± 4.5 mV/s (Figure 4C) and APD_{50} from 37 ± 5.4 to 46.2 ± 5.5 ms (Figure 4D) in SAN myocytes. These effects of Mil on SAN myocytes were fully reversible. In contrast to the SAN, Mil had no effect on AP properties in mouse right atrial myocytes. APD_{50} (8.9 ± 1 vs. 9.4 ± 1), APD_{70} (16.9 ± 2 vs. 18.2 ± 2.3) and APD_{90} (45.7 ± 4.2 vs. 46 ± 4.3) were not different ($P = 0.79$; Figure 4F) upon application of Mil. These data indicate that the mouse SAN has constitutive PDE3 activity that regulates spontaneous AP firing but that PDE3 inhibition does not modulate atrial AP properties in basal conditions.

The effects of the PDE4 inhibitor Rol on AP firing in mouse SAN and right atrial myocytes were measured next (Figure 5, Tables S7 and S8). Rol increased ($P < 0.05$) spontaneous AP frequency in SAN myocytes from 130 ± 8 to 170 ± 9 APs/min (Figure 5B). In addition, Rol increased ($P < 0.05$) DD slope (23.9 ± 1.8 mV/s vs. 44.3 ± 4.3 mV/s; Figure 5C) and APD_{50} (37.5 ± 5 ms vs. 47.8 ± 6.3 ms; Figure 5D) in SAN myocytes. Rol also increased ($P < 0.05$) AP duration in right atrial myocytes (Figure 5F). Specifically, APD_{50} was increased from 9.4 ± 1.7 to 12.9 ± 2 ms, APD_{70} was increased from 19.9 ± 3.4 to 27.4 ± 3.9 ms, and APD_{90} was increased from 51.1 ± 5.9 to 59.1 ± 5.5 ms. These data show that constitutive PDE4 activity contributes to the regulation of AP firing in mouse SAN and atrial myocytes.
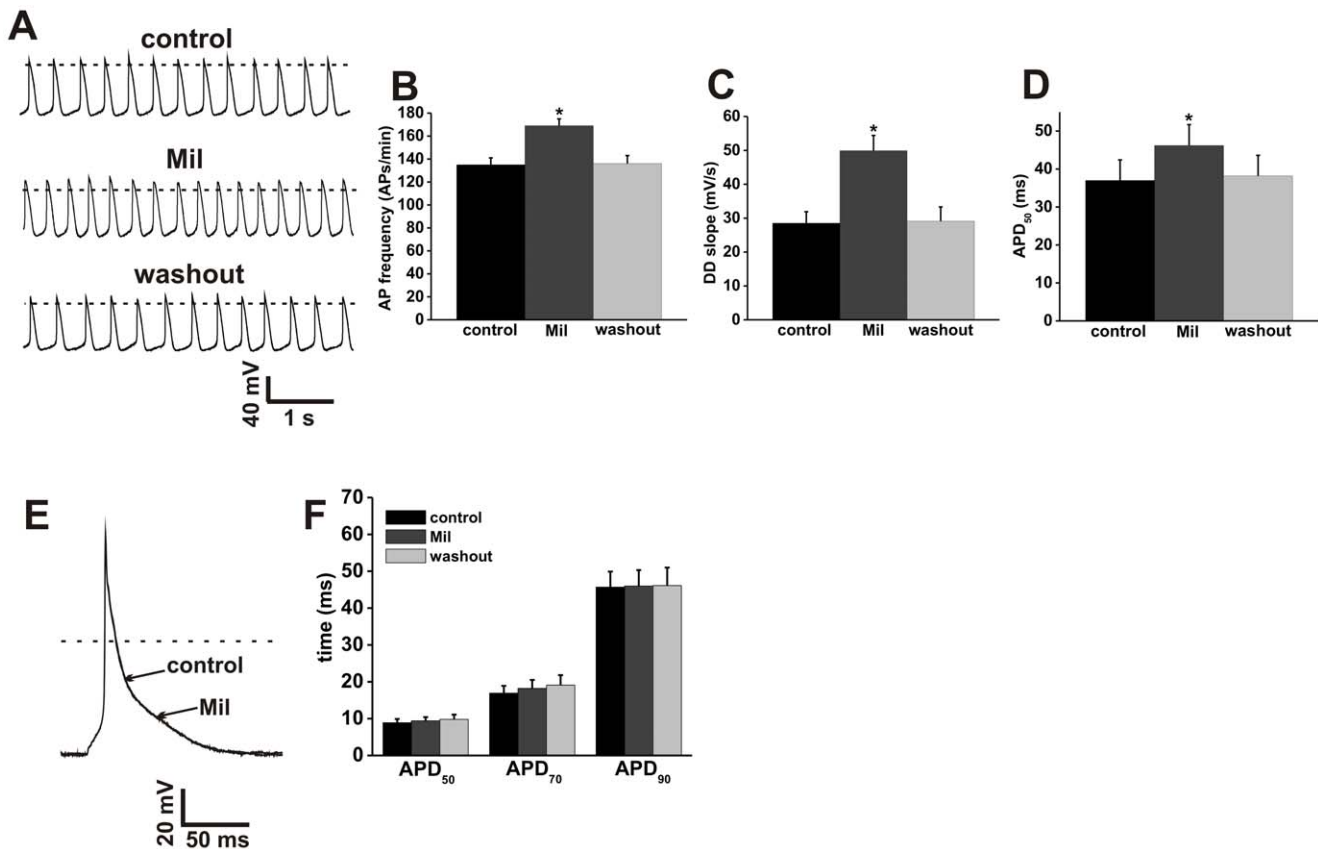
Figure 4. Effects of the PDE3 inhibitor milrinone on action potential firing in SAN and atrial myocytes. A. Representative spontaneous AP recordings (5 s duration) in control conditions, in the presence of Mil (10 µM) and after Mil washout. Dotted lines are at 0 mV. Summary bar graphs illustrate the effects of Mil on spontaneous AP frequency (**B**), DD slope (**C**) and APD$_{50}$ (**D**). **E.** Representative stimulated right atrial myocyte APs in control conditions, in the presence of Mil (10 µM) and after Mil washout. Dotted line is at 0 mV. **F.** Summary of the effects of Mil on atrial AP duration (APD$_{50}$, APD$_{70}$, and APD$_{90}$). Summary data are means ± SEM; $n = 9$ SAN myocytes and 9 right atrial myocytes; *$P < 0.05$ vs. control by one way ANOVA with Tukey's posthoc test.
doi:10.1371/journal.pone.0047652.g004

## Effects of PDE inhibition on L-type Ca^{2+} current in SAN and right atrial myocytes

Numerous studies have demonstrated that I$_{Ca,L}$ is a major target of regulation by PDEs, including PDE2, 3 and 4 [10,11,25,27,28] Furthermore, I$_{Ca,L}$ is a critical determinant of spontaneous AP firing in the SAN [15–17] as well as AP duration in working atrial and ventricular myocytes [18,29,30]. Thus, we next studied the effects of PDE inhibitors on I$_{Ca,L}$ in mouse SAN and right atrial myocytes. For comparison purposes, we also measured I$_{Ca,L}$ in right ventricular myocytes. Importantly, some differences exist in SAN, atrial and ventricular I$_{Ca,L}$. Specifically, I$_{Ca,L}$ in SAN and atrial myocytes is generated by both Ca$_V$1.2 and Ca$_V$1.3 channel isoforms [16,17]. This causes total I$_{Ca,L}$ to activate between −60 and −50 mV and I$_{Ca,L}$ I–V curves to peak between −10 and 0 mV. In contrast, ventricular I$_{Ca,L}$ is determined only by Ca$_V$1.2 channels, activates positive to −40 mV and peaks at approximately +10 mV.

The effects of global PDE inhibition with IBMX (100 µM) on SAN and right atrial myocyte I$_{Ca,L}$ are illustrated in Figure 6. Summary I–V curves demonstrate that IBMX increased ($P < 0.05$) peak I$_{Ca,L}$ density from −4.4±0.3 to −11.2±1 (Figure 6B) in SAN myocytes. The effects of IBMX on SAN myocyte I$_{Ca,L}$ were further studied using steady state conductance analysis (Figure 6C). IBMX increased ($P < 0.05$) I$_{Ca,L}$ maximum conductance (G$_{max}$) from 103.9±6.4 to 225.1±5.9 pS/pF and shifted ($P < 0.05$) the V$_{1/}$

$_{2(act)}$ from −28.4±0.4 to −33.3±0.5 mV. There was no change ($P = 0.588$) in slope factor (6.4±0.6 mV in control vs. 6.3±0.3 mV in IBMX). Similarly, in right atrial myocytes, IBMX increased peak I$_{Ca,L}$ density from −3.9±0.2 to −9.7±0.4 pA/pF (Figure 6E). Steady state conductance analysis in atrial myocytes (Figure 6F) shows that IBMX increased ($P < 0.05$) I$_{Ca,L}$ G$_{max}$ from 112.8±8.8 to 195.8±10.4 pS/pF and shifted ($P < 0.05$) the V$_{1/2(act)}$ from −9.1±1.2 to −18.7±1.1 mV.

The effects of IBMX (100 µM) on I$_{Ca,L}$ in right ventricular myocytes are illustrated in Figure S1. Summary I–V curves show that IBMX increased ($P < 0.05$) peak I$_{Ca,L}$ density from −4.9±0.7 to −11.2±0.9 pA/pF (Figure S1B) in ventricular myocytes. Furthermore, I$_{Ca,L}$ G$_{max}$ in ventricular myocytes was increased ($P < 0.05$) from 115±15.2 to 197.1±23 pS/pF and V$_{1/2(act)}$ was shifted ($P < 0.05$) from −8.9±0.8 to −15.4±1 mV (Figure S1C) in IBMX. Thus, global PDE inhibition potently, and similarly, increases basal I$_{Ca,L}$ in all regions of the myocardium we have investigated.

Next we measured the effects of the PDE2 inhibitor EHNA (10 µM) on SAN and right atrial myocyte I$_{Ca,L}$ (Figure 7). In SAN myocytes EHNA increased ($P < 0.05$) peak I$_{Ca,L}$ density from −4.7±0.4 to −6.1±0.5 pA/pF (Figure 7B). Steady state conductance analysis illustrates that EHNA increased ($P < 0.05$) I$_{Ca,L}$ G$_{max}$ from 106.0±7.7 to 125.5±5.2 pS/pF and shifted the V$_{1/2(act)}$ from −25.1±1.5 to −28.5±1.6 mV (Figure 7C). In right
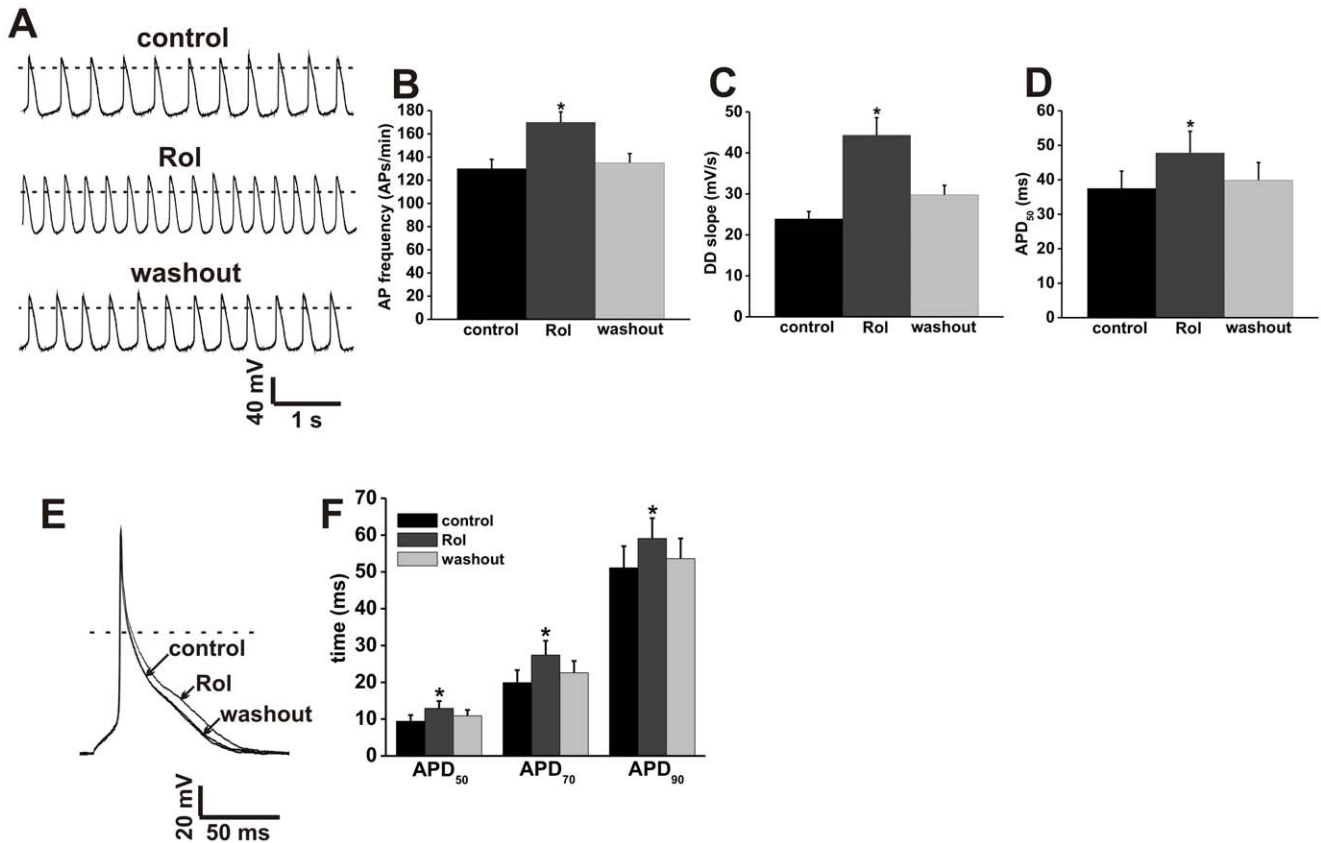
Figure 5. Effects of the PDE4 inhibitor rolipram on action potential firing in SAN and atrial myocytes. A. Representative spontaneous AP recordings (5 s duration) in control conditions, in the presence of Rol (10 μM) and after Rol washout. Dotted lines are at 0 mV. Summary bar graphs illustrate the effects of Rol on spontaneous AP frequency (**B**), DD slope (**C**) and APD$_{50}$ (**D**). **E.** Representative stimulated right atrial myocyte APs in control conditions, in the presence of Rol (10 μM) and after Rol washout. Dotted line is at 0 mV. **F.** Summary of the effects of Rol on atrial AP duration (APD$_{50}$, APD$_{70}$, and APD$_{90}$). Summary data are means ± SEM; $n = 10$ SAN myocytes and 7 right atrial myocytes; *$P<0.05$ vs. control by one way ANOVA with Tukey's posthoc test.
doi:10.1371/journal.pone.0047652.g005

atrial myocytes EHNA increased ($P<0.05$) I$_{Ca,L}$ density from -3.4 ± 0.2 to -4.9 ± 0.5 pA/pF (Figure 7E). Furthermore, I$_{Ca,L}$ G$_{max}$ in right atrial myocytes was increased ($P<0.05$) from 72.8 ± 2.3 to 99.9 ± 3.2 pS/pF by EHNA and the V$_{1/2(act)}$ was shifted ($P<0.05$) from -16.0 ± 1.2 to -18.7 ± 1.4 mV (Figure 7F). These data are consistent with the effects of EHNA on AP properties in SAN and atrial myocytes.

In contrast to SAN and atrial myocytes, EHNA had no effect on right ventricular myocyte I$_{Ca,L}$ (Figure S2). Summary I–V curves (Figure S2B) show no change ($P=0.92$) in I$_{Ca,L}$ density upon application of EHNA. Steady state conductance analysis (Figure S2C) shows that I$_{Ca,L}$ G$_{max}$ (76.3 ± 2.6 pS/pF in control vs. 76.1 ± 2.9 pS/pF in EHNA) and V$_{1/2(act)}$ (-13 ± 1 mV in control vs. -14.4 ± 1.2) were not altered ($P=0.85$) in the presence of EHNA. Thus, although selective PDE2 inhibition does not affect ventricular myocyte I$_{Ca,L}$, it does increase I$_{Ca,L}$ in SAN and atrial myocytes.

The effects of the PDE3 inhibitor Mil (10 μM) on SAN and right atrial I$_{Ca,L}$ are illustrated in Figure 8. Consistent with its effects on spontaneous AP firing, Mil increased ($P<0.05$) peak I$_{Ca,L}$ density in SAN myocytes from -3.8 ± 0.5 to -6.3 ± 0.2 pA/pF (Figure 8B). Also, I$_{Ca,L}$ G$_{max}$ was increased ($P<0.05$) from 110.7 ± 5.8 to 160.4 ± 3.3 pS/pF and V$_{1/2(act)}$ was shifted ($P<0.05$) from -16.8 ± 2.3 to -18.4 ± 2.1 mV by Mil (Figure 8C). In contrast to SAN myocytes, and in agreement with the absence of

effects of PDE3 inhibition on right atrial AP duration, Mil had no effect on right atrial I$_{Ca,L}$. Summary I–V curves (Figure 8E) show no change ($P=0.66$) in peak I$_{Ca,L}$ density upon application of Mil. Furthermore, I$_{Ca,L}$ G$_{max}$ (95.1 ± 2.9 pS/pF in control vs. 100.9 ± 2.3) and V$_{1/2(act)}$ (-10.4 ± 1.2 mV in control vs. -9.9 ± 0.9 mV in Mil) were not altered following PDE3 inhibition in atrial myocytes.

The effects of Mil on right ventricular myocyte I$_{Ca,L}$ are illustrated in Figure S3. Summary I–V curves show that Mil had no effect ($P=0.63$) on peak I$_{Ca,L}$ density (Figure S3B). Also, I$_{Ca,L}$ G$_{max}$ (87.2 ± 1.8 pS/pF in control vs. 91.3 ± 1.4 pS/pF in Mil) and V$_{1/2(act)}$ (-8.8 ± 0.6 mV in control vs. -9.2 ± 0.4 mV in Mil) were not affected ($P=0.52$) by Mil (Figure S3C). Together, these data show that PDE3 inhibition alone markedly increases I$_{Ca,L}$ in the specialized pacemaker myocytes of the SAN, but has no effect on I$_{Ca,L}$ in working atrial or ventricular myocytes.

The effects of PDE4 inhibition with Rol (10 μM) on SAN and right atrial myocyte I$_{Ca,L}$ are presented in Figure 9. In SAN myocytes Rol increased ($P<0.05$) peak I$_{Ca,L}$ density from -4.2 ± 0.1 to -8.1 ± 1.1 pA/pF (Figure 9B). Rol also increased ($P<0.05$) I$_{Ca,L}$ G$_{max}$ from 99.2 ± 7.2 to 188.3 ± 2.8 pS/pF and shifted ($P<0.05$) the V$_{1/2(act)}$ from -18.1 ± 3.1 to -20.2 ± 0.7 mV (Figure 9C). In right atrial myocytes Rol increased ($P<0.05$) peak I$_{Ca,L}$ density from -4.5 ± 0.4 to -7.5 ± 0.7 pA/pF (Figure 9E). Furthermore, Rol increased ($P<0.05$) I$_{Ca,L}$ G$_{max}$ from 130.8 ± 0.7
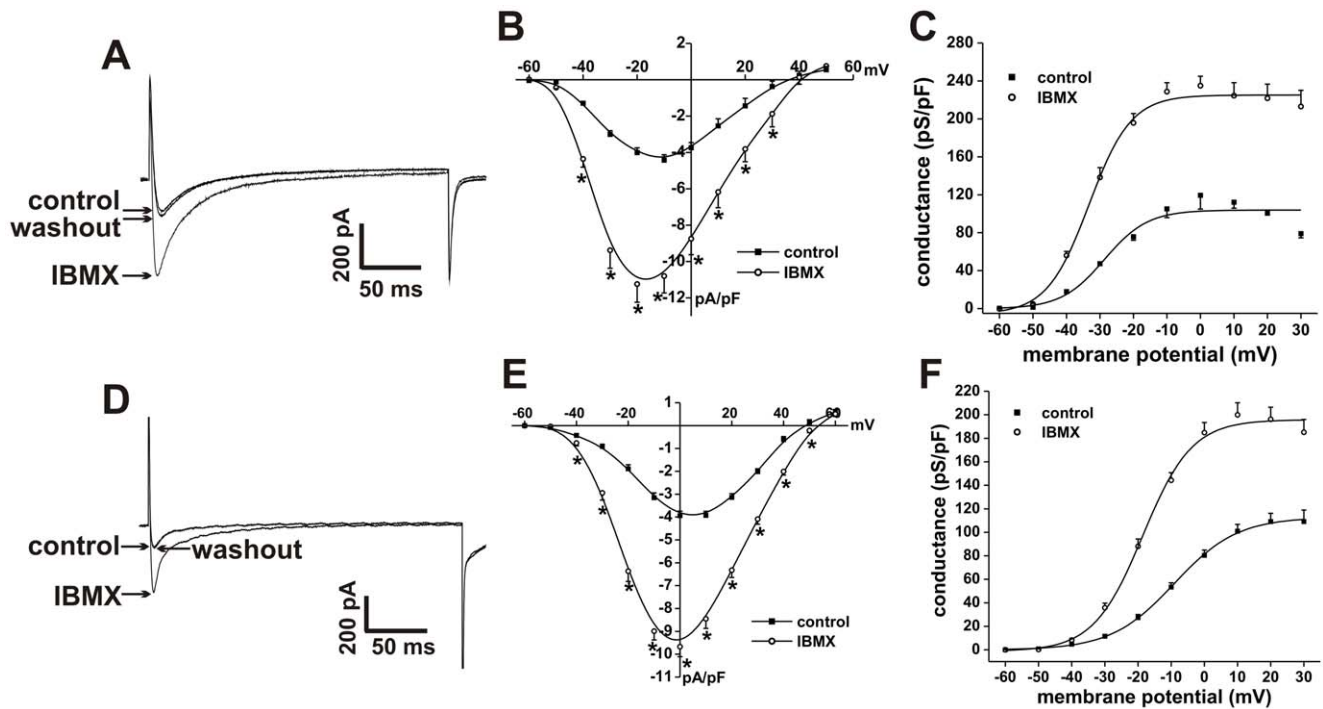
Figure 6. Effects of IBMX on L-type Ca^{2+} current in SAN and right atrial myocytes. A. Representative $I_{Ca,L}$ recordings in SAN myocytes in control conditions, in the presence of IBMX (100 μM) and following IBMX washout. **B.** Summary I–V relationships for the effects of IBMX on SAN myocyte $I_{Ca,L}$. **C.** Summary $I_{Ca,L}$ conductance density plots for the effects of IBMX in SAN myocytes. **D.** Representative $I_{Ca,L}$ recordings in right atrial myocytes in control conditions, in the presence of IBMX (100 μM), and following IBMX washout. **E.** Summary I–V relationships for the effects of IBMX on right atrial myocyte $I_{Ca,L}$. **F.** Summary $I_{Ca,L}$ conductance density plots for the effects of IBMX in right atrial myocytes. Summary data are means ± SEM; $n = 8$ SAN myocytes and 12 right atrial myocytes; *$P < 0.05$ vs. control by paired Student's t-test.
doi:10.1371/journal.pone.0047652.g006

to 176.9±1.0 pS/pF and shifted ($P < 0.05$) the $V_{1/2(act)}$ from −7.1±0.2 to −12.3±0.2 mV (Figure 9F). These effects of PDE4 inhibition on $I_{Ca,L}$ are consistent with the ability of Rol to augment spontaneous AP firing in SAN myocytes and AP duration in atrial myocytes.

In contrast to SAN and atrial myocytes, Rol had no effect on right ventricular myocyte $I_{Ca,L}$ (Figure S4). Summary I–V curves illustrate no change ($P = 0.13$) in peak $I_{Ca,L}$ density following application of Rol. In addition, neither $I_{Ca,L}$ G_{max} (98.5±1.5 pS/pF in control vs. 95.1±1.9 pS/pF in Rol) or $V_{1/2(act)}$ (−9.1±0.4 mV in control vs. −8.9±0.6) were modulated ($P = 0.53$) by Rol. Thus, selective PDE4 inhibition elicits increases in $I_{Ca,L}$ in SAN and atrial myocytes, but not in ventricular myocytes.

The observation that selective PDE inhibitors, when given alone, have no effect on basal $I_{Ca,L}$ in ventricular myocytes is consistent with previous studies in mice and rats, which have shown that selective inhibitors must be given in combination to augment basal $I_{Ca,L}$ [10,11]. We have confirmed this pattern in our experiments by demonstrating that combined inhibition of PDE3 and PDE4 with Mil and Rol increases right ventricular myocyte $I_{Ca,L}$ (Figure S5). Summary I–V curves illustrate that Mil + Rol increased peak $I_{Ca,L}$ density (−4.5±0.3 pA/pF in control vs. −6.7±0.6 pA/pF in Mil + Rol; $P < 0.05$), increased $I_{Ca,L}$ G_{max} (84.8±1.5 pS/pF in control vs. 105.5±3.9 pS/pF in Mil + Rol; $P < 0.05$) and shifted the $V_{1/2(act)}$ (−11.2±0.5 mV in control vs. −20.8±1.1 mV in Mil + Rol; $P < 0.05$) compared to control. Thus, our data illustrating the effects of global and specific PDE inhibitors on ventricular $I_{Ca,L}$ fully agree with previous studies, which supports the conclusion that specific PDE inhibitors have

distinct effects in different regions of the myocardium. These ventricular $I_{Ca,L}$ data also confirm that the PDE inhibitors we have used are selective at the doses we have studied. We also measured the effects of combined PDE3/4 inhibition on AP firing and $I_{Ca,L}$ in SAN and right atrial myocytes. We observed that Mil + Rol augments AP firing and $I_{Ca,L}$ in SAN and atrial myocytes similarly to IBMX (data not shown).

Discussion

PDEs are critical regulators of cAMP and cGMP levels in cardiomyocytes, representing the primary enzymes responsible for cyclic nucleotide degradation, and acting as the only counter balance to the mechanisms responsible for cyclic nucleotide production (adenylyl and guanylyl cyclases) [1,2]. In this study, we have measured the effects of global (IBMX) and specific (EHNA, Mil, Rol) PDE inhibitors on AP firing and $I_{Ca,L}$ in mouse SAN and atrial myocytes. We also measured the effects of these inhibitors on mouse ventricular $I_{Ca,L}$ in order to make direct comparisons between the three myocyte types. This is the first direct comparison of these effects in the mouse myocardium. The main finding of these experiments is that PDE effects on AP firing and basal $I_{Ca,L}$ are distinct in the different regions of the myocardium.

Our AP data clearly demonstrate that global PDE inhibition with IBMX potently increases spontaneous AP frequency in mouse SAN myocytes in association with increases in DD slope and APD_{50}. Similarly IBMX markedly increased AP duration at 50, 70 and 90% repolarization in mouse atrial myocytes. These data show that there is a high level of constitutive PDE activity that regulates AP properties in the SAN and atrial myocardium; however, subsequent experiments with specific PDE inhibitors
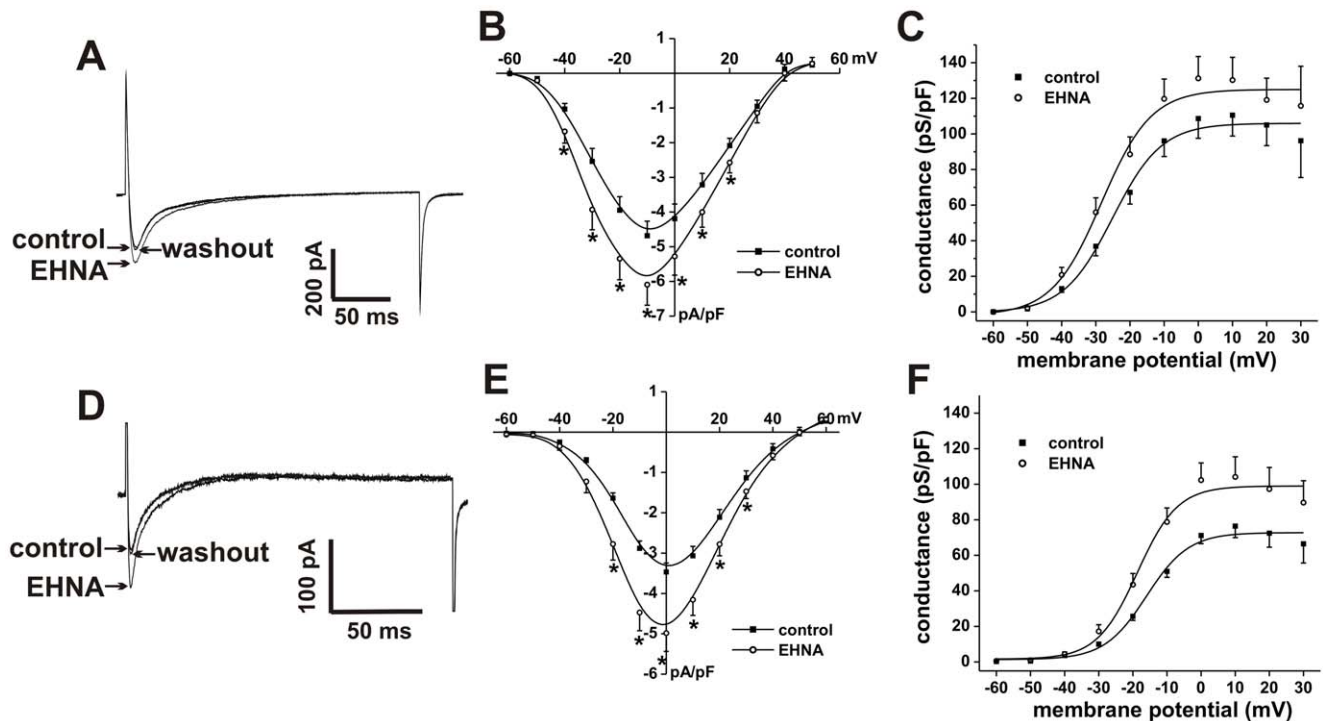
Figure 7. Effects of the PDE2 inhibitor EHNA on L-type Ca^{2+} current in SAN and right atrial myocytes. A. Representative I$_{Ca,L}$ recordings in SAN myocytes in control conditions, in the presence of EHNA (10 µM) and following EHNA washout. **B.** Summary I–V relationships for the effects of EHNA on SAN myocyte I$_{Ca,L}$. **C.** Summary I$_{Ca,L}$ conductance density plots for the effects of EHNA in SAN myocytes. **D.** Representative I$_{Ca,L}$ recordings in right atrial myocytes in control conditions, in the presence of EHNA (10 µM), and following EHNA washout. **E.** Summary I–V relationships for the effects of EHNA on right atrial myocyte I$_{Ca,L}$. **F.** Summary I$_{Ca,L}$ conductance density plots for the effects of EHNA in right atrial myocytes. Summary data are means ± SEM; $n = 6$ SAN myocytes and 10 right atrial myocytes; *$P<0.05$ vs. control by paired Student's t-test.
doi:10.1371/journal.pone.0047652.g007

revealed important differences between the two cell types. Specifically, in mouse SAN myocytes, EHNA, Mil and Rol each increased spontaneous AP frequency on their own, indicating that PDE2, PDE3 and PDE4 all contribute to the regulation of AP properties in basal conditions. In contrast, in mouse atrial myocytes, only EHNA and Rol were able to increase AP duration whereas Mil had no effect, indicating that constitutive PDE2 and PDE4, but not PDE3 activity, regulates atrial AP properties.

Similar trends were also observed for I$_{Ca,L}$ in SAN and atrial myocytes. Specifically, IBMX increased basal I$_{Ca,L}$ by approximately 185% in SAN myocytes and 140% in atrial myocytes. Consistent with our AP measurements, SAN myocyte I$_{Ca,L}$ was increased by each of the selective inhibitors EHNA (~31%), Mil (~66%) and Rol (~93%). In atrial myocytes only EHNA (~38%) and Rol (~72%) increased basal I$_{Ca,L}$. Mil had no significant effect on right atrial I$_{Ca,L}$ once again confirming a key difference between SAN and atrial myocytes in terms of which specific PDE inhibitors are able to modulate basal AP properties and I$_{Ca,L}$ in mice.

For further comparison, we measured the effects of IBMX on basal I$_{Ca,L}$ in mouse right ventricular myocytes and observed increases of approximately 130%. In agreement with prior studies [8,10,11], but in contrast to our findings in SAN and atrial myocytes, none of the selective PDE inhibitors we tested had any effect on basal I$_{Ca,L}$ in ventricular myocytes. Only when Mil and Rol were applied together was ventricular I$_{Ca,L}$ increased as also noted previously [11]. Thus, although IBMX potently and similarly increases I$_{Ca,L}$ in all regions of the myocardium, the ability of selective PDE inhibitors (EHNA, Mil or Rol) to modulate

basal I$_{Ca,L}$ is strikingly different in SAN, atrial and ventricular myocytes.

We also measured the mRNA expression of specific isoforms from the PDE2, PDE3 and PDE4 family in SAN, right atrial and right ventricular myocardium using quantitative PCR. These data show that PDE2A, PDE3A, PDE3B, PDE4A, PDE4B and PDE4D are all expressed in each region of the myocardium and that several differences exist in expression levels between SAN, right atrium and right ventricular free wall. Note that these specific isoforms were chosen based on prior studies that have shown these same isoforms are detectable in atrial and ventricular myocardium or isolated ventricular myocytes [7,11,31]. Comparing our electrophysiological data with our mRNA expression data suggests the differences in ability of specific PDE inhibitors to modulate AP firing and basal I$_{Ca,L}$ in the different regions of the myocardium are not strictly related to differences in expression. For example, PDE2A is similarly expressed in each region of the myocardium yet PDE2 inhibition with EHNA augments I$_{Ca,L}$ in SAN and atrial myocytes, but not ventricular myocytes. Also, PDE3A (thought to be the main PDE3 isoform in cardiac myocytes [32,33]) is lowest in the SAN and highest in the ventricular myocardium; however, PDE3 inhibition with Mil only modulates basal I$_{Ca,L}$ in SAN myocytes. Thus, it is likely that factors other than expression levels contribute importantly to the different effects of selective PDE inhibitors in different regions of the heart. These could include differences in subcellular localization of PDEs by anchoring proteins, differences in basal adenylyl and guanylyl cyclase activities, and differences in activity of PDE regulatory proteins in SAN, atrial and ventricular myocytes. It should also be noted that mRNA levels do not necessarily correlate with protein levels
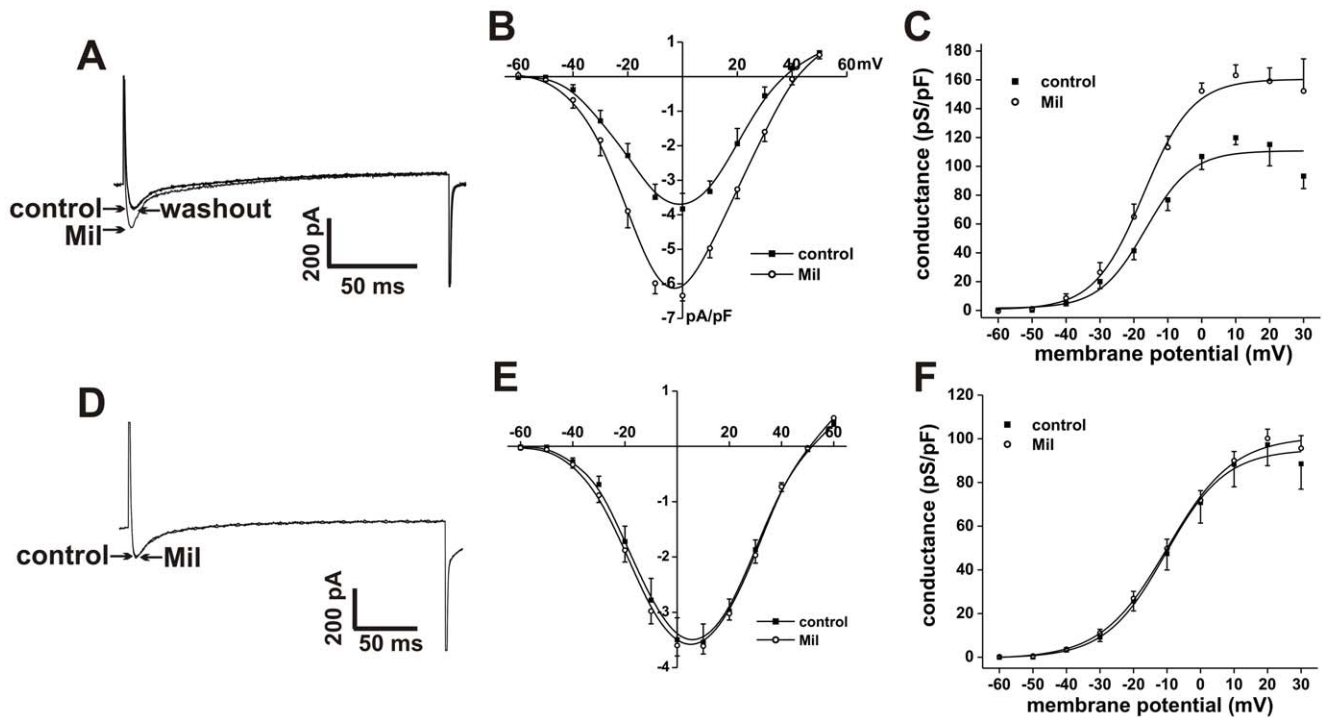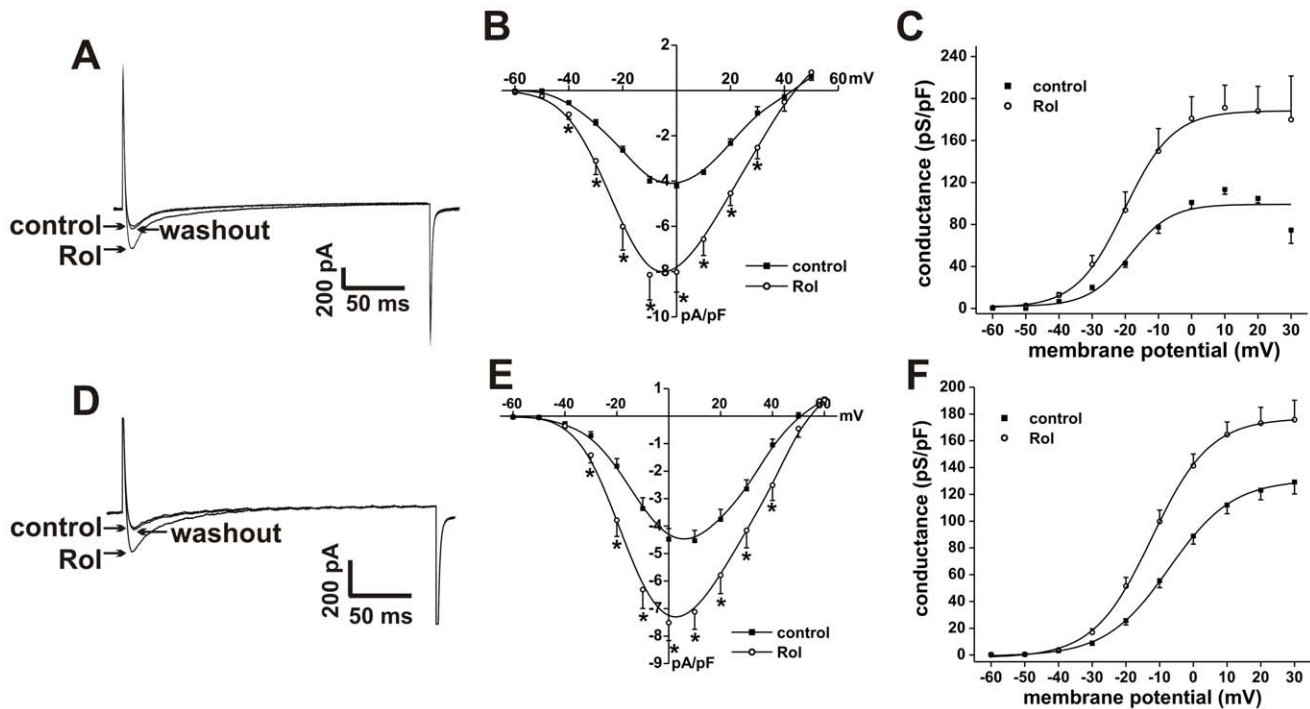
Figure 8. Effects of the PDE3 inhibitor milrinone on L-type Ca^{2+} current in SAN and right atrial myocytes. A. Representative I$_{Ca,L}$ recordings in SAN myocytes in control conditions, in the presence of Mil (10 µM) and following Mil washout. **B.** Summary I–V relationships for the effects of Mil on SAN myocyte I$_{Ca,L}$. **C.** Summary I$_{Ca,L}$ conductance density plots for the effects of Mil in SAN myocytes. **D.** Representative I$_{Ca,L}$ recordings in right atrial myocytes in control conditions, in the presence of Mil (10 µM), and following Mil washout. **E.** Summary I–V relationships for the effects of Mil on right atrial myocyte I$_{Ca,L}$. **F.** Summary I$_{Ca,L}$ conductance density plots for the effects of Mil in right atrial myocytes. Summary data are means ± SEM; $n = 6$ SAN myocytes and 12 right atrial myocytes; *$P < 0.05$ vs. control by paired Student's t-test.
doi:10.1371/journal.pone.0047652.g008

and/or enzymatic activity. Our mRNA measurements were done at the tissue level thus, in addition to myocytes, other cell types, such as cardiac fibroblasts, would be expected to be present in these samples and may contribute to total PDE mRNA levels. Further studies will therefore be required to better understand the basis for the differences in effects of PDE inhibitors in each region of the myocardium.

As our study represents the first direct comparison of different PDE inhibitors on electrophysiological responses in SAN, atrial and ventricular myocytes in mice it is useful to compare our data with those reported in studies that have mainly used other species. Few studies have characterized the effects of PDE inhibitors in the specialized SAN; however, one recent report [34] did demonstrate the effects of various PDE inhibitors on spontaneous AP frequency in rabbit SAN myocytes. This study showed that PDE3 was the major constitutively active PDE in the basal state in rabbit, with Mil increasing AP frequency almost as effectively as IBMX. Other PDE inhibitors, including EHNA and Rol had much smaller effects. This is different from what we have observed in the mouse in which Mil and Rol each had similar stimulatory effects on AP frequency and where the stimulatory effect of EHNA, although smaller than Mil and Rol, was still robust. Other studies have also shown that PDE3 inhibitors increase SAN AP frequency in rabbits [35] and guinea pigs [36]; however, these studies did not compare these effects with inhibitors of other PDE families. Our data showing that PDE3 and PDE4 inhibitors can similarly increase AP frequency and I$_{Ca,L}$ in mouse SAN myocytes are consistent with studies showing these inhibitors also increase beating rate in mouse and rat atrial preparations [37].

Several studies have measured the effects of selective PDE inhibitors on I$_{Ca,L}$ in human atrial myocytes and these findings can be compared to our observations in mouse right atrial myocytes. Similar to our findings in mouse atrial myocytes, inhibition of PDE2 with EHNA potentiates basal I$_{Ca,L}$ in human atrial myocytes [27] indicating that PDE2 regulates basal I$_{Ca,L}$ in both mouse and human atrium. In contrast, whereas we found no effect of Mil on basal I$_{Ca,L}$ in mouse atrial myocytes, PDE3 inhibition does increase basal I$_{Ca,L}$ in human atrial myocytes [28,38]. Recently, PDE4 has also been shown to regulate basal cAMP levels in human atrial myocytes using a fluorescence resonance energy transfer based reporter system [39] suggesting that PDE4 likely regulates basal I$_{Ca,L}$ in human atrium as it does in mice. This would be consistent with data indicating that the role of PDE4 in cAMP regulation is conserved between human and rodent hearts [31].

Our experiments have focused on the PDE2, 3 and 4 families and on the role of I$_{Ca,L}$ in mediating changes in AP properties in SAN and atrial myocytes. This was done in order to facilitate comparisons and highlight differences with the effects of PDE inhibitors on ventricular I$_{Ca,L}$. Although the changes in AP properties we observed in SAN and atrial myocytes correlated very well with changes in I$_{Ca,L}$ it is likely that other ionic mechanisms contribute as well. For example, the hyperpolarization-activated current (I$_f$) contributes prominently to the DD in SAN myocytes and is well known to be directly modulated by cAMP [13,15]. We have shown that PDE3 inhibition with Mil increases basal I$_f$ in mouse SAN myocytes [20] and it has also been shown that IBMX increases I$_f$ in rabbit SAN myocytes [40]. Also, the slope of the DD in SAN myocytes is partly determined by Ca^{2+} release from the SR and a subsequent activation of the Na$^+$-Ca^{2+} exchanger (I$_{NCX}$) [12]. This

Figure 9. Effects of the PDE4 inhibitor rolipram on L-type Ca²⁺ current in SAN and right atrial myocytes. A. Representative I$_{Ca,L}$ recordings in SAN myocytes in control conditions, in the presence of Rol (10 μM) and following Rol washout. **B.** Summary I–V relationships for the effects of Rol on SAN myocyte I$_{Ca,L}$. **C.** Summary I$_{Ca,L}$ conductance density plots for the effects of Rol in SAN myocytes. **D.** Representative I$_{Ca,L}$ recordings in right atrial myocytes in control conditions, in the presence of Rol (10 μM), and following Rol washout. **E.** Summary I–V relationships for the effects of Rol on right atrial myocyte I$_{Ca,L}$. **F.** Summary I$_{Ca,L}$ conductance density plots for the effects of Rol in right atrial myocytes. Summary data are means ± SEM; n = 6 SAN myocytes and 12 right atrial myocytes; *P<0.05 vs. control by paired Student's t-test.
doi:10.1371/journal.pone.0047652.g009

SR Ca²⁺ release mechanism is also cAMP sensitive and has been shown to be constitutively regulated by PDE3 [34]. Other possible targets include cyclic nucleotide sensitive delayed rectifier K⁺ currents, such as I$_{Ks}$, which can be modulated by IBMX and Mil in guinea pig SAN myocytes [41]. It is not known if mouse SAN expresses I$_{Ks}$, but it has been shown to express I$_{Kr}$ channels that are thought to be cAMP sensitive [42]. Further studies will be needed to assess the possible contributions of each of these ionic currents to the changes in AP properties elicited by PDE inhibitors in mouse SAN. Interestingly, spontaneous AP firing in the SAN is also partially determined by a T-type Ca²⁺ current (I$_{Ca,T}$) [15,43,44]. Numerous studies have shown that I$_{Ca,T}$, including in SAN myocytes, is not modulated by cAMP [43,45–48]; thus, it is unlikely that I$_{Ca,T}$ is affected by PDE inhibitors.

It is also possible that other PDE families contribute to AP and ionic current regulation in SAN and atrial myocytes. For example, PDE1 and PDE5 have been shown to be expressed in the heart and to play functional roles in some settings [1,7,49,50]. More recently PDE8 has also been identified in ventricular myocardium [7]. Whether these PDE families have distinct roles in SAN or atrial myocytes in mice is yet to be determined.

In summary, we have characterized the effects of inhibitors of PDE2, PDE3 and PDE4 on AP properties in mouse SAN and atrial myocytes and directly compared the effects of these inhibitors on basal I$_{Ca,L}$ in SAN, right atrial and right ventricular myocytes. Although IBMX potently increased I$_{Ca,L}$ in all cell types our data demonstrate that each region of the myocardium displays a unique pattern of response to family specific PDE inhibitors. SAN myocytes were responsive to each specific inhibitor tested, while atrial myocytes were responsive to PDE2 and PDE4, but not

PDE3 inhibitors. Ventricular myocytes, on the other hand, do not respond to any family specific PDE inhibitors when given alone. These differences may be important when considering cyclic nucleotide regulation of ion channels in different regions of the heart. It is now known that PDE signaling in the heart is complex, based on the hypothesis that PDEs can be compartmentalized to distinct subcellular regions. Our data show that another aspect of the complexity of PDE regulation in the heart is related to regional differences in the roles of specific PDE families on ion channel regulation in the SAN compared to the working (atrial and ventricular) myocardium.

Supporting Information

Figure S1 Effects of IBMX on L-type Ca²⁺ current in right ventricular myocytes. A. Representative I$_{Ca,L}$ recordings (at 0 mV from −40 mV) in right ventricular myocytes in control conditions, in the presence of IBMX (100 μM), and after IBMX washout. **B.** Summary I–V relationships for the effects of IBMX on right ventricular I$_{Ca,L}$. **C.** Summary I$_{Ca,L}$ conductance density plots for the effects of IBMX on right ventricular myocytes. Summary data are means ± SEM; n = 6 ventricular myocytes; *P<0.05 vs. control by paired Student's t-test.
(TIF)

Figure S2 Effects of PDE2 inhibition with EHNA on L-type Ca²⁺ current in right ventricular myocytes. A. Representative I$_{Ca,L}$ recordings (at 0 mV from −40 mV) in right ventricular myocytes in control conditions, in the presence of EHNA (10 μM), and after EHNA washout. **B.** Summary I–V relationships for the effects of EHNA on right ventricular I$_{Ca,L}$. **C.**

Summary $I_{Ca,L}$ conductance density plots for the effects of EHNA on right ventricular myocytes. Summary data are means ± SEM; $n = 10$ ventricular myocytes; EHNA had no effect on right ventricular $I_{Ca,L}$ (paired Student's t-test).
(TIF)

Figure S3 Effects of PDE3 inhibition with milrinone on L-type Ca^{2+} current in right ventricular myocytes. A. Representative $I_{Ca,L}$ recordings (at 0 mV from −40 mV) in right ventricular myocytes in control conditions, in the presence of Mil (10 µM), and after Mil washout. **B.** Summary I–V relationships for the effects of Mil on right ventricular $I_{Ca,L}$. **C.** Summary $I_{Ca,L}$ conductance density plots for the effects of Mil on right ventricular myocytes. Summary data are means ± SEM; $n = 5$ ventricular myocytes; Mil had no effect on right ventricular $I_{Ca,L}$ (paired Student's t-test).
(TIF)

Figure S4 Effects of PDE4 inhibition with rolipram on L-type Ca^{2+} current in right ventricular myocytes. A. Representative $I_{Ca,L}$ recordings (at 0 mV from −40 mV) in right ventricular myocytes in control conditions, in the presence of Rol (10 µM), and after Rol washout. **B.** Summary I–V relationships for the effects of Rol on right ventricular $I_{Ca,L}$. **C.** Summary $I_{Ca,L}$ conductance density plots for the effects of Rol on right ventricular myocytes. Summary data are means ± SEM; $n = 5$ ventricular myocytes; Rol had no effect on right ventricular $I_{Ca,L}$ (paired Student's t-test).
(TIF)

Figure S5 Effects of PDE3 and PDE4 inhibition with milrinone and rolipram on L-type Ca^{2+} current in right ventricular myocytes. A. Representative $I_{Ca,L}$ recordings (at 0 mV from −40 mV) in right ventricular myocytes in control conditions, in the presence of Mil + Rol (10 µM each), and after drug washout. **B.** Summary I–V relationships for the effects of Mil + Rol on right ventricular $I_{Ca,L}$. **C.** Summary $I_{Ca,L}$ conductance density plots for the effects of Mil + Rol on right ventricular myocytes. Summary data are means ± SEM; $n = 8$ ventricular myocytes; $*P < 0.05$ vs. control by paired Student's t-test.
(TIF)

Appendix S1 Supplemental materials and methods.
(PDF)

Table S1 Effects of IBMX on spontaneous action potential parameters in isolated mouse SAN myocytes.
(PDF)

Table S2 Effects of IBMX on stimulated action potential parameters in isolated mouse right atrial myocytes.
(PDF)

Table S3 Effects of EHNA on spontaneous action potential parameters in isolated mouse SAN myocytes.
(PDF)

Table S4 Effects of EHNA on stimulated action potential parameters in isolated mouse right atrial myocytes.
(PDF)

Table S5 Effects of milrinone on spontaneous action potential parameters in isolated mouse SAN myocytes.
(PDF)

Table S6 Effects of milrinone on stimulated action potential parameters in isolated mouse right atrial myocytes.
(PDF)

Table S7 Effects of rolipram on spontaneous action potential parameters in isolated mouse SAN myocytes.
(PDF)

Table S8 Effects of rolipram on stimulated action potential parameters in isolated mouse right atrial myocytes.
(PDF)

Author Contributions

Conceived and designed the experiments: RH AA RAR. Performed the experiments: RH AA CR GR RAR. Analyzed the data: RH AA CR GR RAR. Contributed reagents/materials/analysis tools: RAR. Wrote the paper: RH AA CR RR.

References

1. Bender AT, Beavo JA (2006) Cyclic nucleotide phosphodiesterases: molecular regulation to clinical use. Pharmacol Rev 58:488–520.
2. Omori K, Kotera J (2007) Overview of PDEs and their regulation. Circ Res 100:309–327.
3. Maurice DH, Palmer D, Tilley DG, Dunkerley HA, Netherton SJ, et al. (2003) Cyclic nucleotide phosphodiesterase activity, expression, and targeting in cells of the cardiovascular system. Mol Pharmacol 64:533–546.
4. Fischmeister R, Castro LR, Abi-Gerges A, Rochais F, Jurevicius J, et al. (2006) Compartmentation of cyclic nucleotide signaling in the heart: the role of cyclic nucleotide phosphodiesterases. Circ Res 99:816–828.
5. Movsesian MA (2002) PDE3 cyclic nucleotide phosphodiesterases and the compartmentation of cyclic nucleotide-mediated signalling in cardiac myocytes. Basic Res Cardiol 97 Suppl 1:I83–I90.
6. Zaccolo M (2011) Spatial control of cAMP signalling in health and disease. Curr Opin Pharmacol 11:649–655.
7. Patrucco E, Albergine MS, Santana LF, Beavo JA (2010) Phosphodiesterase 8A (PDE8A) regulates excitation-contraction coupling in ventricular myocytes. J Mol Cell Cardiol 49:330–333.
8. Fischmeister R, Hartzell HC (1991) Cyclic AMP phosphodiesterases and Ca^{2+} current regulation in cardiac cells. Life Sci 48:2365–2376.
9. Mongillo M, Tocchetti CG, Terrin A, Lissandron V, Cheung YF, et al. (2006) Compartmentalized phosphodiesterase-2 activity blunts beta-adrenergic cardiac inotropy via an NO/cGMP-dependent pathway. Circ Res 98:226–234.
10. Kerfant BG, Zhao D, Lorenzen-Schmidt I, Wilson LS, Cai S, et al. (2007) PI3K? is required for PDE4, not PDE3, activity in subcellular microdomains containing the sarcoplasmic reticulum calcium ATPase in cardiomyocytes. Circ Res 101:400–408.
11. Verde I, Vandecasteele G, Lezoualc'h F, Fischmeister R (1999) Characterization of the cyclic nucleotide phosphodiesterase subtypes involved in the regulation of the L-type Ca^{2+} current in rat ventricular myocytes. Br J Pharmacol 127:65–74.
12. Lakatta EG, Maltsev VA, Vinogradova TM (2010) A coupled SYSTEM of intracellular Ca^{2+} clocks and surface membrane voltage clocks controls the timekeeping mechanism of the heart's pacemaker. Circ Res 106:659–673.
13. DiFrancesco D (1993) Pacemaker mechanisms in cardiac tissue. Annu Rev Physiol 55:455–472.
14. Irisawa H, Brown HF, Giles W (1993) Cardiac pacemaking in the sinoatrial node. Physiol Rev 73:197–227.
15. Mangoni ME, Nargeot J (2008) Genesis and regulation of the heart automaticity. Physiol Rev 88:919–982.
16. Mangoni ME, Couette B, Bourinet E, Platzer J, Reimer D, et al. (2003) Functional role of L-type Cav1.3 Ca^{2+} channels in cardiac pacemaker activity. Proc Natl Acad Sci U S A 100:5543–5548.
17. Zhang Z, Xu Y, Song H, Rodriguez J, Tuteja D, et al. (2002) Functional Roles of Cav1.3 (a1D) calcium channel in sinoatrial nodes: insight gained using gene-targeted null mutant mice. Circ Res 90:981–987.
18. Nerbonne JM, Kass RS (2005) Molecular physiology of cardiac repolarization. Physiol Rev 85:1205–1253.
19. Zhang Z, He Y, Tuteja D, Xu D, Timofeyev V, et al. (2005) Functional roles of Cav1.3 (a1D) calcium channels in atria: insights gained from gene-targeted null mutant mice. Circulation 112:1936–1944.
20. Springer J, Azer J, Hua R, Robbins C, Adamczyk A, et al. (2012) The natriuretic peptides BNP and CNP increase heart rate and electrical conduction by stimulating ionic currents in the sinoatrial node and atrial myocardium following activation of guanylyl cyclase-linked natriuretic peptide receptors. J Mol Cell Cardiol 52:1122–1134.

21. Cifelli C, Rose RA, Zhang H, Voigtlaender-Bolz J, Bolz SS, et al. (2008) RGS4 Regulates Parasympathetic Signaling and Heart Rate Control in the Sinoatrial Node. Circ Res 103:527–535.

22. Rose RA, Lomax AE, Kondo CS, Anand-Srivastava MB, Giles WR (2004) Effects of C-type natriuretic peptide on ionic currents in mouse sinoatrial node: a role for the NPR-C receptor. Am J Physiol 286:H1970–H1977.

23. Rose RA, Sellan M, Simpson JA, Izaddoustdar F, Cifelli C, et al. (2011) Iron Overload Decreases CaV1.3-Dependent L-Type Ca^{2+} Currents Leading to Bradycardia, Altered Electrical Conduction, and Atrial Fibrillation. Circ Arrhythm Electrophysiol 4:733–742.

24. Marionneau C, Couette B, Liu J, Li H, Mangoni ME, et al. (2005) Specific pattern of ionic channel gene expression associated with pacemaker activity in the mouse heart. J Physiol 562:223–234.

25. Mery PF, Pavoine C, Pecker F, Fischmeister R (1995) Erythro-9-(2-hydroxy-3-nonyl)adenine inhibits cyclic GMP-stimulated phosphodiesterase in isolated cardiac myocytes. Mol Pharmacol 48:121–130.

26. Lugnier C (2006) Cyclic nucleotide phosphodiesterase (PDE) superfamily: a new target for the development of specific therapeutic agents. Pharmacol Ther 109:366–398.

27. Rivet-Bastide M, Vandecasteele G, Hatem S, Verde I, Benardeau A, et al. (1997) cGMP-stimulated cyclic nucleotide phosphodiesterase regulates the basal calcium current in human atrial myocytes. J Clin Invest 99:2710–2718.

28. Vandecasteele G, Verde I, Rucker-Martin C, Donzeau-Gouge P, Fischmeister R (2001) Cyclic GMP regulation of the L-type Ca^{2+} channel current in human atrial myocytes. J Physiol 533:329–340.

29. Bers DM, Perez-Reyes E (1999) Ca channels in cardiac myocytes: structure and function in Ca influx and intracellular Ca release. Cardiovasc Res 42:339–360.

30. Marban E (2002) Cardiac channelopathies. Nature 415:213–218.

31. Richter W, Xie M, Scheitrum C, Krall J, Movsesian MA, et al. (2011) Conserved expression and functions of PDE4 in rodent and human heart. Basic Res Cardiol 106:249–262.

32. Beca S, schars-Sobbi R, Panama BK, Backx PH (2011) Regulation of murine cardiac function by phosphodiesterases type 3 and 4. Curr Opin Pharmacol 11:714–719.

33. Kerfant BG, Rose RA, Sun H, Backx PH (2006) Phosphoinositide 3-kinase? Regulates Cardiac Contractility by Locally Controlling Cyclic Adenosine Monophosphate Levels. Trends Cardiovasc Med 16:250–256.

34. Vinogradova TM, Sirenko S, Lyashkov AE, Younes A, Li Y, et al. (2008) Constitutive phosphodiesterase activity restricts spontaneous beating rate of cardiac pacemaker cells by suppressing local Ca^{2+} releases. Circ Res 102:761–769.

35. Hata T, Nishimura M, Ogino K, Uchiyama H, Watanabe Y (1998) Electrophysiological effects of amrinone on the automaticity and membrane current system of the rabbit sinoatrial node cells. Heart Vessels 13:114–121.

36. Orito K, Takase H, Fujiki H, Mori T (1996) Effects of toborinone (OPC-18790), a new positive inotropic agent, on action potential in guinea pig sinoatrial node: compared with milrinone and E-4031. Jpn J Pharmacol 72:79–82.

37. Kaumann AJ (2011) Phosphodiesterases reduce spontaneous sinoatrial beating but not the 'fight or flight' tachycardia elicited by agonists through Gs-protein-coupled receptors. Trends Pharmacol Sci 32:377–383.

38. Kirstein M, Rivet-Bastide M, Hatem S, Benardeau A, Mercadier JJ, et al. (1995) Nitric oxide regulates the calcium current in isolated human atrial myocytes. J Clin Invest 95:794–802.

39. Molina CE, Leroy J, Richter W, Xie M, Scheitrum C, et al. (2012) Cyclic adenosine monophosphate phosphodiesterase type 4 protects against atrial arrhythmias. J Am Coll Cardiol 59:2182–2190.

40. DiFrancesco D, Tromba C (1988) Muscarinic control of the hyperpolarization-activated current (if) in rabbit sino-atrial node myocytes. J Physiol 405:493–510.

41. Shimizu K, Shintani Y, Ding WG, Matsuura H, Bamba T (2002) Potentiation of slow component of delayed rectifier K^{+} current by cGMP via two distinct mechanisms: inhibition of phosphodiesterase 3 and activation of protein kinase G. Br J Pharmacol 137:127–137.

42. Clark RB, Mangoni ME, Lueger A, Couette B, Nargeot J, et al. (2004) A rapidly activating delayed rectifier K^{+} current regulates pacemaker activity in adult mouse sinoatrial node cells. Am J Physiol Heart Circ Physiol 286:H1757–H1766.

43. Hagiwara N, Irisawa H, Kameyama M (1988) Contribution of two types of calcium currents to the pacemaker potentials of rabbit sino-atrial node cells. J Physiol 395:233–253.

44. Mangoni ME, Traboulsie A, Leoni AL, Couette B, Marger L, et al. (2006) Bradycardia and slowing of the atrioventricular conduction in mice lacking CaV3.1/a1G T-type calcium channels. Circ Res 98:1422–1430.

45. Bean BP (1985) Two kinds of calcium channels in canine atrial cells. Differences in kinetics, selectivity, and pharmacology. J Gen Physiol 86:1–30.

46. Ertel SI, Ertel EA, Clozel JP (1997) T-type Ca^{2+} channels and pharmacological blockade: potential pathophysiological relevance. Cardiovasc Drugs Ther 11:723–739.

47. Hess P (1988) Elementary properties of cardiac calcium channels: a brief review. Can J Physiol Pharmacol 66:1218–1223.

48. Hirano Y, Fozzard HA, January CT (1989) Characteristics of L- and T-type Ca^{2+} currents in canine cardiac Purkinje cells. Am J Physiol 256:H1478–H1492.

49. Vandeput F, Wolda SL, Krall J, Hambleton R, Uher L, et al. (2007) Cyclic nucleotide phosphodiesterase PDE1C1 in human cardiac myocytes. J Biol Chem 282:32749–32757.

50. Zhang M, Kass DA (2011) Phosphodiesterases and cardiac cGMP: evolving roles and controversies. Trends Pharmacol Sci 32:360–365.